SAND--98-8479C

Chemical Response of Methane/Air Diffusion Flames to Unsteady Strain Rate*

LOUF-980804--

HONG G. IM and JACQUELINE H. CHEN
Combustion Research Facility
Sandia National Laboratories, Livermore, CA 94551-0969

JYH-YUAN CHEN
Department of Mechanical Engineering
University of California, Berkeley, CA 94720-1740

Corresponding author:
Dr. Hong G. Im
Combustion Research Facility, MS 9051
Sandia National Laboratories
Livermore, CA 94551-0969, USA

Phone: (510) 294-3131
Fax: (510) 294-2595
email: hgim@ca.sandia.gov

Word Count:
Text: 3360 (estimate 320 words/page × 10.5 pages)
Table: 100
Figures 1-4,7-8: 1200 (6 × 200)
Figure 5: 600 (2-column, 1/2 page)
Figure 6: 300 (1-column)
Total: 5560

Preferred Presentation:
Oral

Preferred colloquium topic area:
Laminar Flame Dynamics, Pollutant Formation

*Submitted to the 27th Symposium (International) on Combustion, Boulder, CO, August 2-7, 1998.

DISCLAIMER

Abstract

Effects of unsteady strain rate on the response of methane/air diffusion flames are studied. We use the finite-domain opposed flow configuration in which the nozzle exit velocity is imposed as a function of time. The GRI mechanism v2.11 is used for the detailed methane/air chemistry. The response of individual species to monochromatic oscillation in strain rate with various frequencies reveals that the fluctuation of slow species, such as CO and NO_x, is more rapidly suppressed as the flow time scale decreases. It is also observed that the maximum CO concentration is very insensitive to the variation in the scalar dissipation rate. An extinction event due to an abrupt imposition of high strain rates is also simulated by an impulsive velocity with various frequencies. For a fast impulse, a substantial overshoot in NO_2 concentration is observed after extinction. Finally, the overall fuel burning rate shows a nonmonotonic response to the variation in characteristic unsteady time scale, while the emission indices for NO_x shows monotonic decay in response as frequency is increased.

Introduction

Unsteady effects on laminar flamelets have recently attracted significant research effort due to its relevance and potential importance in further understanding of turbulent combustion. While previous studies of steady opposed flames demonstrated good agreement with many experimental observations such as extinction limits and the laminar flame speed, there are still some discrepancies that may be attributed to either experimental inaccuracy or to the limitation of the steady-flame assumption. One such result is the experimental study by Masri *et al.* [1] in which the Raman measurement of turbulent methane/air diffusion flames showed that the maximum CO concentration far exceeds the numerical predictions with strained laminar flames. Chen and Dibble [2] attempted to describe such an observation based on the perfectly-stirred-reaction (PSR) model, suggesting some possibility of excessive CO due to the extinction/re-ignition process, while a one-dimensional flamelet calculation by Barlow and Chen [3] showed only a minimal change in the temperature and species profiles. It may be conjectured that the PSR combustion can sustain a much wider range of residence time scales than the flamelet configuration since PSR is only controlled by reaction which has much shorter time scales than diffusion. The present study attempts to further investigate this unsteadiness issue in an opposed jet configuration which has been commonly adopted in experimental studies. It also provides a more complete description of the strained laminar flamelet behavior in the presence of convective terms.

A number of studies have recently been performed regarding the basic flame behavior in an opposed jet configuration subjected to oscillatory strain rates[4-9]. Some common observations from these studies may be summarized as follows: (1) the flame response is attenuated as the frequency of the imposed oscillation increases, (2) the flame response becomes more sensitive near the extinction limit, and as a consequence of (1), it can be said that (3) the flame is more resistant to extinction for high frequency such that the laminar

flamelet regime is expected to be valid over a wider range of turbulent Reynolds numbers. The main motivation of the present study is to extend these findings to the response of individual chemical species to unsteady strain rates. Since the key reaction steps for different species all have different time scales, when subjected to unsteady flows it is expected that the response of one species will deviate from another, which may in turn lead to a description of flamelets quite different from that in the quasi-steady limit.

Two types of flow unsteadiness are considered: an oscillatory velocity with different frequencies and an impulsive velocity forcing with various characteristic rise times. The former provides clear information regarding phase and amplitude response to the characteristic frequency, while the latter may be more relevant in representing the interaction of flamelets with turbulent eddies. In particular, the focus of the study is on the response of major pollutant species including CO and NO_x.

Governing Equations and Numerical Method

We adopt the system of an axisymmetric, opposed jet configuration where two impinging nozzles are separated by a finite distance. Using the boundary layer approximation in the axial direction, the conservation equations for mass, radial and axial momentum, energy and species along the centerline of symmetry are written as [10]:

$$\frac{\partial \rho}{\partial t} + \frac{\partial}{\partial x}(2F) - 2G = 0, \tag{1}$$

$$\frac{\partial G}{\partial t} + 2\frac{\partial}{\partial x}\left(\frac{FG}{\rho}\right) - \frac{3G^2}{\rho} - H(t) - \frac{\partial}{\partial x}\left[\mu\frac{\partial}{\partial x}\left(\frac{G}{\rho}\right)\right] = 0, \tag{2}$$

$$\rho\frac{\partial T}{\partial t} + 2F\frac{\partial T}{\partial x} - \frac{1}{c_p}\frac{\partial}{\partial x}\left(\lambda\frac{\partial T}{\partial x}\right) - \frac{\partial p}{\partial t} + \frac{\rho}{c_p}(\sum_k c_p Y_k V_k)\frac{\partial T}{\partial x} + \frac{1}{c_p}\sum_k h_k W_k \omega_k = 0, \tag{3}$$

$$\rho\frac{\partial Y_k}{\partial t} + 2F\frac{\partial Y_k}{\partial x} + \frac{\partial}{\partial x}(\rho Y_k V_k) - W_k\omega_k = 0, \quad k = 1, \cdots, K, \tag{4}$$

where $F(x,t) = \rho u/2$, $G(x,t) = -\rho v/r = -\rho(\partial v/\partial r)$, and the radial pressure gradient, $H(t) = (1/r)(\partial p/\partial r)$, is an eigenvalue of the problem. The remainder of the nomenclature follows that of Kee *et al.* [11].

In this formulation, the axial and radial velocity components at the nozzle exit can be independently specified and the pressure eigenvalue is computed as a solution. We impose the plug-flow condition and thus the boundary conditions are:

$$x = 0: \quad F = \frac{\rho_F u_F(t)}{2}, \quad G = 0, \quad T = T_F, \quad Y_k = (Y_k)_F, \tag{5}$$

$$x = L: \quad F = -\frac{\rho_O u_O(t)}{2}, \quad G = 0, \quad T = T_O, \quad Y_k = (Y_k)_O, \tag{6}$$

where the velocity at both nozzle exits are maintained symmetric such that $u_F(t) = -u_O(t)$ for all time. The thermodynamic pressure variation is not considered in this study, so $\partial p/\partial t = 0$.

Equations (1)–(4) are solved numerically with detailed methane/air chemistry [12]. The numerical code for the steady problem, OPPDIF [13], has been modified to accomodate the unsteady equations. The new unsteady code, named OPUS (OPposed-jet Unsteady Strain), uses the same spatial differencing as that of OPPDIF while time integration is performed with the differential-algebraic system solver, DASSL [14]. A steady solution field obtained from OPPDIF with further mesh refinement is used as the initial condition for the unsteady problem.

We study the axisymmetric counterflow system with pure methane against air, thereby forming a diffusion flame. The nozzle separation is set to 1 cm. The temperature at the nozzle exits is held constant at 300 K and pressure is 1 atm. The strain rate, κ, is defined as the maximum velocity gradient $(\partial u/\partial x)$ on the oxidizer side, and the scalar dissipation rate at the stoichiometric mixture fraction is defined as

$$\chi_{st} = (2\alpha|\nabla\xi|^2)_{\xi=\xi_{st}}, \tag{7}$$

where $\alpha = \lambda/\rho c_p$ is the thermal diffusivity and the mixture fraction, ξ, is based on a linear combination of elemental mass fractions [15]. The two quantities κ and χ_{st}, computed from the instantaneous solution field *a posteriori*, have been interchangeably used in many steady flame studies. However, in an unsteady problem it is not clear whether they still correlate, scine the two quantities are evaluated at different locations in space. This issue will be examined in the next section.

Figure 1 shows steady S-curve responses of the maximum flame temperature, strain rate and stoichiometric scalar dissipation rate as a function of the imposed velocity. At the extinction turning point, it is found that $T_f = 1785$ K, $\kappa = 535$ s^{-1} and $\chi_{st} = 19.8$ s^{-1}. It appears that, for this steady response both κ and χ_{st} correlate fairly well with u_F, with κ being more linearly correlated with u_F than χ_{st}.

A steady solution field chosen at a specific u_F value in Fig. 1 is used as the initial condition, u_0, for the unsteady problem. Then the unsteady boundary condition is imposed as

$$u_F(t) = -u_O(t) = u_0 \mathcal{F}(t). \tag{8}$$

We shall study two functional forms of $\mathcal{F}(t)$:

$$\mathcal{F}(t) = 1 + A[1 - \cos(2\pi f t)] \tag{9}$$

for the oscillatory case, and

$$\mathcal{F}(t) = 1 + A \exp[-4f(t - t_0)^2] \tag{10}$$

for the impulsive case. Here A is the fractional amplitude of the velocity fluctuation with respect to its initial value, and f is the frequency (for the oscillatory case) or the inverse of the characteristic rise time (for the impulsive case). Results are presented predominantly for the oscillatory case in terms of the physico-chemical response of the flames to the flow unsteadiness, while only some key results are highlighted for the impulsively forced case.

Results and Discussion

Response to Oscillatory Flows

From the steady response shown in Fig. 1, we choose $u_0 = 100\text{cm/s}$ and $A = 0.23$ such that the flame approaches the steady extinction limit at the point of maximum velocity for slow oscillations. First, it is of interest to observe how the strain rate and scalar dissipation rate follow the imposed velocity oscillation. Figure 2 shows the response of κ and χ_{st} to the imposed velocity $u_F(t)$ after the limit cycles are achieved. The reference steady response is also shown in this figure as denoted by the dotted line. The degree of tilting and roundness of the ellipses with respect to the steady curve provide information regarding amplitude decay and phase delay of the unsteady response. Comparing the two figures, it appears that the scalar dissipation rate is a better parameter for characterizing the unsteady flow field response since the low frequency result ($10\ \text{s}^{-1}$) follows the steady result more closely, and the phase response is monotonic. To substantiate this point, the phase delays for various quantities with respect to the imposed velocity oscillation are presented in Fig. 3. The phase delay of each variable is defined as the difference in the phase angle relative to its own quasi-steady response. Consistent with previous results [8, 16], it is observed that the phase delay of κ is nonmonotonic, while the phase delay of χ_{st} increases monotonically. Since κ is evaluated at a location far into the oxidizer side, it can be expected that the unsteady flow response at that location would be out of phase with the flow at the reaction zone for certain frequencies. Therefore, although κ defined as such may be convenient for comparison with experiment, the scalar dissipation rate appears to be a better indicator of what occurs at the instantaneous reaction zone, and is a more relevant parameter in the context of turbulent nonpremixed combustion.

To proceed with the study of unsteady response of chemical species, we first define ap-

propriate characteristic time scales for individual species. Noting that, in the reaction zone,

$$\frac{\partial X_k}{\partial t} \approx \omega_k, \tag{11}$$

the chemical time scale for species k can be defined as

$$\tau_k = \frac{X_{k,max}}{\omega_{k,max}}, \tag{12}$$

where the subscript *max* denotes the spatial maximum value. We can further decompose the characteristic times by dividing ω_k into production and consumption rates depending on the direction of the elementary reactions. Table 1 shows the results for several species determined from the steady solution used as the initial condition in the study. It is readily noted that the characteristic time scales for CO and NO_x species are much longer than those for most of the major radicals. It can be generally stated that, as the frequency of the imposed unsteadiness increases, the amplitude of the response becomes attenuated and the phase delay is increased due to the inability of the reaction zone to readily adjust to the imposed unsteady fluctuation. Therefore, those species with longer characteristic chemical times are expected to exhibit a larger value of the phase delay and faster attenuation in amplitude. The phase and amplitude response of various species, presented in Figs. 3 and 4, show exactly the expected behavior, *i.e.* the response of NO_x decays faster and lags further than temperature and major radicals (OH, H). The response of CO is also consistent except for the nonmonotonic behavior of the amplitude response which will be discussed later. It is interesting to note that the response of temperature is almost identical to that of OH and H.

We have also identified the various pathways for the NO_x formation by a method similar to Nishioka *et al.* [17]. For the range of scalar dissipation rates studied here, we find that the Zeldovich and N_2O paths represent only a few percent of the total NO production, consistent with previous studies for steady diffusion flames [17, 18]. Therefore, the NO

behavior presented herein can be understood as primarily that of prompt NO. It is of interest to note from Table 1 that the time scales for production and consumption of HCN, the main precursor of the prompt NO, are very close to those of NO.

Figure 5 shows the phase diagram of the maximum mole fraction of various species as a function of χ_{st} for three different frequencies. It is seen that OH (Fig. 5(a)) follows the steady response curve without significant phase lag, *i.e.* the amplitude decrease in OH is mainly due to the decay in the scalar dissipation rate response to the imposed velocity oscillation. We also find that the flame temperature responds in a similar fashion to OH, as also observed in Figs. 3 and 4. The response of NO and NO_2 (Figs. 5(a) and 5(d)) is similar, but a substantial increase in phase delay and amplitude decay with respect to χ_{st} is noted. For $f = 1000\ s^{-1}$, NO_2 shows almost no response to the imposed unsteady strain rate.

The behavior of CO shown in Fig. 5(b) needs further discussion. It should first be noted that even the steady-state response of CO concentration is distinctively nonmonotonic. This is due to the disparity in the characteristic times for production and consumption rates of CO, as shown in Table 1. That is, the main CO consumption reaction, CO + OH = CO_2 + H, has a relatively longer time scale. Therefore, as the scalar dissipation rate increases, the reduced residence time for CO consumption leads to an increase in its concentration. As the scalar dissipation rate is further increased to a point near extinction, however, all of the chemical rates are suppressed and the temperature suddenly decreases, leading to a decrease in the maximum CO concentration. Therefore, for the low frequency oscillation ($10\ s^{-1}$), the maximum CO concentration is limited by the peak value in the steady response curve; in terms of time response, this leads to a dual-peak response in the maximum CO concentration. For higher frequencies, however, the range of the effective scalar dissipation rate is reduced due to the unsteadiness. Coupled with the phase delay, for $f = 100\ s^{-1}$ the maximum CO concentration is actually larger than the steady maximum value. Consequently, the total

amplitude of the oscillation in the maximum CO concentration increases with frequency and then decreases, as shown in Fig. 4.

Despite this unique behavior of CO, however, we also note that the overall magnitude of the changes in the maximum CO concentration is surprisingly small compared to other species. This result is consistent with recent experimental observation in turbulent jet diffusion flames [19], which show good overall agreement between turbulent and laminar strained flame data over a substantial range of turbulent Reynolds numbers. Therefore, it may be concluded that CO is one of the least sensitive species in a strained diffusion flame, and the earlier experimental observation of excessive CO [1] may only be explained via the PSR concept, in which extremely strong turbulence may cause continual local extinction/reignition processes within the turbulent flame brush.

Response to Impulsive Flows

In this section we study the flame response to the impulsive velocity field given by Eq. (10), which may be more relevant to turbulence-flame interaction whereby laminar flamelets are subjected to intermittent impulses of strain produced by turbulent eddies. The Gaussian function in Eq. (10) was chosen such that the characteristic rise time of the burst is about $1/f$, which is a major parameter of the study. The same initial condition ($u_0 = 100$ cm/s) as in the oscillatory case is used.

The species response to the impulsive velocity forcing was found to be consistent with that to the oscillatory flow, simply by interpreting $1/f$ as the characteristic time scale for the unsteady flow field. Therefore, in this section we only present the transient response of species during the extinction process.

Two representative cases are presented in Fig. 6, (a) slow ($f = 10$ s^{-1}) and (b) fast impulse ($f = 1000$ s^{-1}). For each case, the amplitude of velocity fluctuation, A, has been

adjusted to ensure that the maximum χ_{st} is above the extinction limit. For the slow impulse case (a), the flame responds to the unsteady flow in a quasi-steady manner, such that a slight increase in the maximum CO concentration is achieved prior to extinction, while OH and NO decrease monotonically, all consistent with the steady behavior shown in Fig. 5. It is also observed that NO (whose time scale is longer) decreases earlier than OH in a more gradual manner, indicating a more sensitive response to the scalar dissipation rate in a quasi-steady limit. On the other hand, for a faster impulse (b), due to the reduced unsteady time scale, the slower species, such as CO and NO, do not respond to the impulsive flow immediately and thus further lag faster species like OH. Furthermore, these slow species exhibit longer tails in time after OH is completely extinguished. It is noted that, during this extinction period, we observe a large overshoot of NO_2 concentration, which is attributed to the conversion of NO to NO_2 caused by the flame quenching [21].

We further examine the reaction response in terms of the overall production or consumption rate of species for various unsteady time scales. In this case, we use the initial value of $u_0 = 120$ cm/s, and fix the value $A = 0.23$ such that the peak value is close to the extinction condition in the quasi-steady limit. Figure 7 shows the temporal change in fuel consumption rate normalized by its initial value. We first remark that, despite the decrease in the maximum temperature and radical concentration, the overall burning (and thus the total heat release) rate increases during the burst. This is a well-known fact for diffusion flames; the more fuel that is supplied, the more it reacts, as long as the flame is not pushed to the extinction limit. Consequently, in Fig. 7 we observe a nonmonotonic behavior of the fuel consumption rate, *i.e.* the maximum value *increases* with f and then eventually decreases for an extremely fast impulse ($f = 1000$ s^{-1}). Therefore, for the parametric cases studied here, there appears to be an optimal unsteady time scale for which the maximum fuel consumption is achieved. This nonmonotonic response in burning rate to frequency is

similar to the results in a previous study with simple one-step chemistry [22].

Finally, for the same conditions as in Fig. 7, we evaluate the emission index of NO_x, which can be defined as [20]:

$$EI_{NO_x} = \frac{1000 \times (W_{NO} \int_{-\infty}^{\infty} \omega_{NO} dx + W_{NO_2} \int_{-\infty}^{\infty} \omega_{NO_2} dx)}{-W_{CH_4} [\int_{-\infty}^{\infty} \omega_{CH_4} dx]_{t=0}} \quad [g/kg], \tag{13}$$

where we choose the denominator to be the initial fuel mass burning rate. The results are shown in Fig. 8 for various characteristic rise times. It is seen that the emission index drops substantially when the high scalar dissipation rate is applied, and this behavior is attenuated substantially as f increases. In view of the opposite results presented in Figs. 7 and 8, it appears that there may exist some range of unsteady turbulent time scales that leads to an optimal state of combustion. Considering the highest sensitivity of NO_x response, however, it is more likely that such an optimal condition would be governed by NO_x production control, and thus slow fluctuations in the flow field are preferred.

Conclusions

The chemical response of strained diffusion flames to unsteady flows is studied in a finite-domain opposed jet configuration using detailed methane/air chemistry, with flow unsteadiness imposed at the nozzle exit. The response of the major pollutants, CO and NO_x, is studied and described in terms of the relative characteristic time scales of the unsteady flow. It is found that the scalar dissipation rate, as commonly used in the description of turbulent nonpremixed flames, is a more appropriate parameter than strain rate to characterize the unsteady flame behavior.

As for the chemical response of the diffusion flame, the phase and amplitude response of individual species demonstrated that, due to the relatively slow time scales, the response of CO and NO_x is more rapidly suppressed as the flow time scale decreases. This tendency is most notable for CO which exhibits a nonmonotonic response in its maximum concentration

to an increase in frequency. However, it was also observed that the maximum CO concentration is least sensitive to changes in the scalar dissipation rate, such that the peculiar nonmonotonic behavior does not appear to be of practical significance. This finding is consistent with a recent experimental study [19], in which most species profiles in a turbulent jet diffusion flame agree very well with laminar flame predictions even for very large turbulent Reynolds numbers.

The results for the impulsive velocity forcing are consistent with those for the oscillatory forcing in terms of the response related to relative time scales between the species and the unsteady flow. For a fast impulse, a substantial overshoot in NO_2 concentration was observed after extinction. Finally, it was found that the overall fuel burning rate shows a nonmonotonic response to the variation in characteristic unsteady time scale, while the emission index for NO_x shows monotonic decay as frequency is increased. Considering the sensitive response of NO_x formation, it appears that a low-frequency velocity fluctuation is more desirable in terms of pollutant control.

Acknowledgment

This research was supported by the United States Department of Energy, Office of Basic Energy Sciences, Chemical Sciences Division. The authors would like to thank Drs. A. E. Lutz, J. F. Grcar of Sandia National Laboratories, and Prof. R. J. Kee of Colorado School of Mines for their helpful comments during the development of the numerical code.

References

[1] Masri, A. R., Bilger, R. W. and Dibble, R. W., *Twenty-Third Symposium (International) on Combustion*, The Combustion Institute, Pittsburgh, PA, 1988, pp. 693-698.

[2] Chen, J.-Y. and Dibble, R. W., *Combust. Sci. Tech.*, 84:45-50 (1991).

[3] Barlow, R. S. and Chen, J.-Y., *Twenty-Fourth Symposium (International) on Combustion*, The Combustion Institute, Pittsburgh, PA, 1992, pp. 231-237.

[4] Darabiha, N., *Combust. Sci. Tech.*, 86:163-181 (1992).

[5] Ghoniem, A. F., Soteriou, M. C. and Knio, O. M., *Twenty-Fourth Symposium (International) on Combustion*, The Combustion Institute, Pittsburgh, PA, 1992, pp. 223-230.

[6] Brown, B. A. and Sohrab, S. H., 1991 Fall Technical Meeting, The Eastern Section of the Combustion Institute, Oct. 14-16, Cornell University, Ithaca, NY, 1991.

[7] Im, H. G., Bechtold, J. K. and Law, C. K., *Combust. Sci. Tech.*, 106:345-361 (1995).

[8] Egolfopoulos, F. N. and Campbell, C. S., *J. Fluid Mech.*, 318:1-29 (1996).

[9] Kistler, J. S., Sung, C. J., Kreutz, T. G., Law, C. K. and Nishioka, M., *Twenty-Sixth Symposium (International) on Combustion*, The Combustion Institute, Pittsburgh, PA, 1996, pp. 113-120.

[10] Stahl, G. and Warnatz, J., *Combust. Flame*, 85:285-299 (1991).

[11] Kee, R. J., Miller, J. A., Evans, G. H. and Dixon-Lewis, G., *Twenty-Second Symposium (International) on Combustion*, The Combustion Institute, Pittsburgh, PA, 1988, pp. 1479-1494.

[12] Frenklach, M., Wang, H., Goldenberg, M., Smith, G. P., Golden, D. M., Bowman, C. T., Hanson, R. K., Gardiner, W. C. and Lissianski, V., "GRI-Mech—An Optimized Detailed Chemical Reaction Mechanism for Methane Combustion," GRI Report No. GRI-95/0058, November 1, 1995.

[13] Lutz, A. E., Kee, R. J., Grcar, J. F. and Rupley, F. M., "OPPDIF: A Fortran Program for Computing Opposed-flow Diffusion Flames," Sandia National Laboratories Report No. SAND96-8243, May 1996.

[14] Petzold, L. R., "A Description of DASSL: A Differential/Algebraic System Solver," Sandia National Laboratories Report No. SAND82-8637, Sept. 1982.

[15] Bilger, R. W., *Twenty-Second Symposium (International) on Combustion*, The Combustion Institute, Pittsburgh, PA, 1988, pp. 475-488.

[16] Sung, C. J. and Law, C. K., *Combust. Sci. Tech.*, in press (1997).

[17] Nishioka, M., Nakagawa, S., Ishikawa, Y. and Takeno, T., *Combust. Flame*, 98:127-138 (1994).

[18] Smooke, M. D., Ern, A., Tanoff, M. A., Valdati, B. A., Mohammed, R. K., Marran, D. F. and M. B. Long, *Twenty-Sixth Symposium (International) on Combustion*, The Combustion Institute, Pittsburgh, PA, 1996, pp. 2161-2170.

[19] Barlow, R. S. and Frank, J. H., *Twenty-Seventh Sympositum (International) on Combustion*, The Combustion Institute, Pittsburgh, PA, submitted (1998).

[20] Takeno, T. and Nishioka, M., *Combust. Flame*, 92:465-468 (1993).

[21] Cernansky, N. P. and Sawyer, R. F., *Fifteenth Symposium (International) on Combustion*, The Combustion Institute, Pittsburgh, PA, 1975, pp. 1039-1050.

[22] Im, H. G., Law, C. K., Kim, J. S. and Williams, F. A., *Combust. Flame*, 100:21-30 (1995).

	OH	H	O	CO	NO	NO_2	HCN
Production	4.21	2.33	6.19	68.5	68.3	45.1	49.2
Consumption	4.61	2.93	5.31	187.4	99.4	36.6	97.0
Net	23.7	7.12	25.5	83.1	94.4	161.1	59.8

Table 1. Characteristic times for selected species for pure methane against air at 300K, for $\chi_{st} = 11.9\text{s}^{-1}$ or $u_0 = 100\text{cm/s}$ as a representative case. Units are in microseconds.

Figure Captions

Figure 1 S-curve response of steady methane/air diffusion flame with GRI v2.11.

Figure 2 Response of (a) the strain rate, κ, and (b) the scalar dissipation rate, χ_{st}, to the imposed nozzle exit velocity, $u_F(t)$, for different oscillation frequencies.

Figure 3 Phase delay of variables with respect to the quasi-steady response as a function of oscillation frequency.

Figure 4 Amplitude of unsteady fluctuation responses normalized by the quasi-steady values as a function of frequency.

Figure 5 Response of the maximum mole fractions of (a) OH, (b) CO, (c) NO and (d) NO_2 to the scalar dissipation rate, for three different frequencies.

Figure 6 Response of the scalar dissipation rate and maximum mole fractions of of various species to the impulsive flow field; (a) $u_0 = 100$ cm/s, $A = 0.6$ and $f = 10$ s^{-1}; (b) $u_0 = 100$ cm/s, $A = 2.4$ and $f = 1000$ s^{-1}.

Figure 7 Normalized fuel consumption rate as a function of time for various values of f for $u_0 = 120$ cm/s and $A = 0.23$. The abscissa is normalized by each characteristic time scale.

Figure 8 Emission index of NO_x as a function of time for various values of f for $u_0 = 120$ cm/s and $A = 0.23$. The abscissa is normalized by each characteristic time scale.

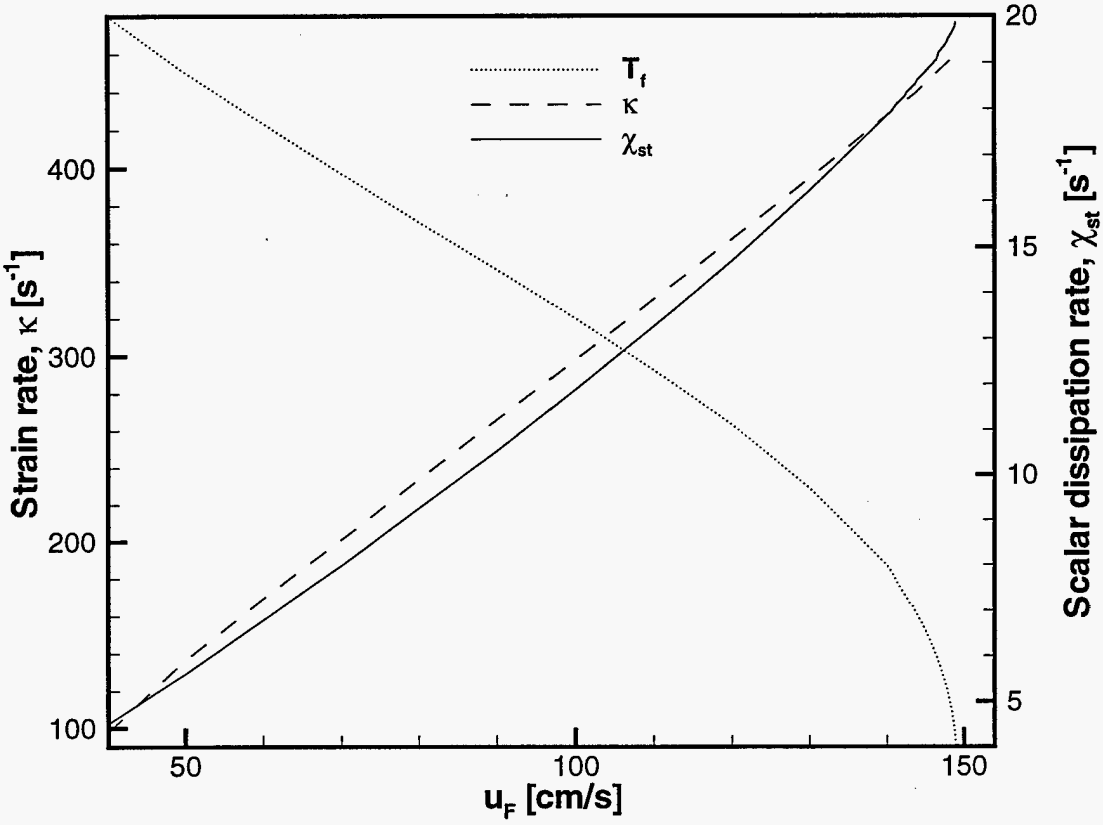

Figure 1: S-curve response of steady methane/air diffusion flame with GRI v2.11.

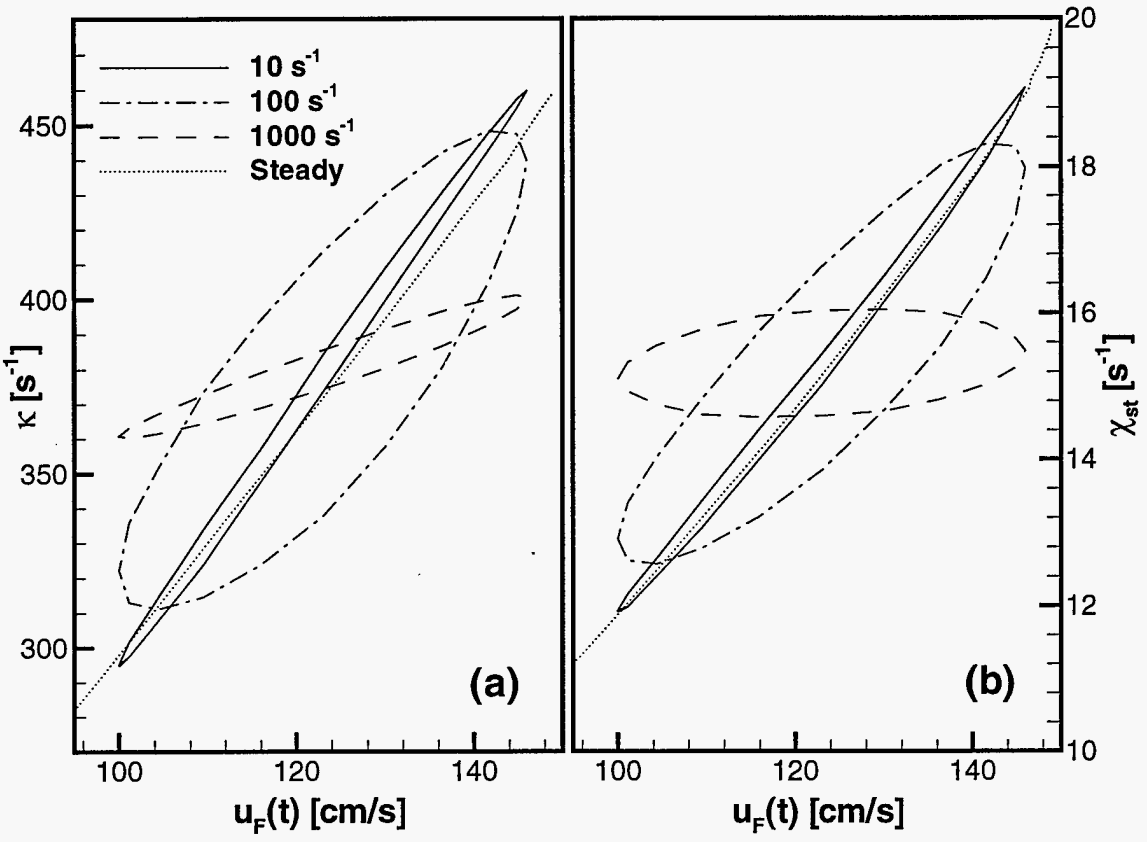

Figure 2: Response of (a) the strain rate, κ, and (b) the scalar dissipation rate, χ_{st}, to the imposed nozzle exit velocity, $u_F(t)$, for different oscillation frequencies.

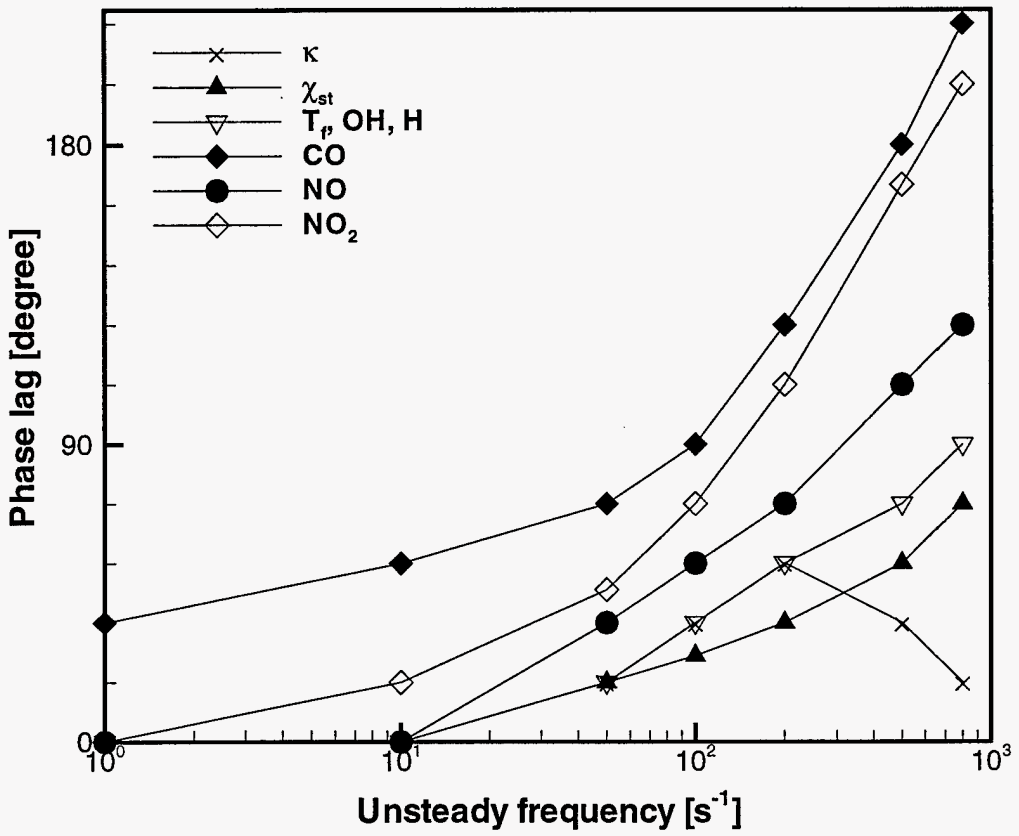

Figure 3: Phase delay of variables with respect to the quasi-steady response as a function of oscillation frequency.

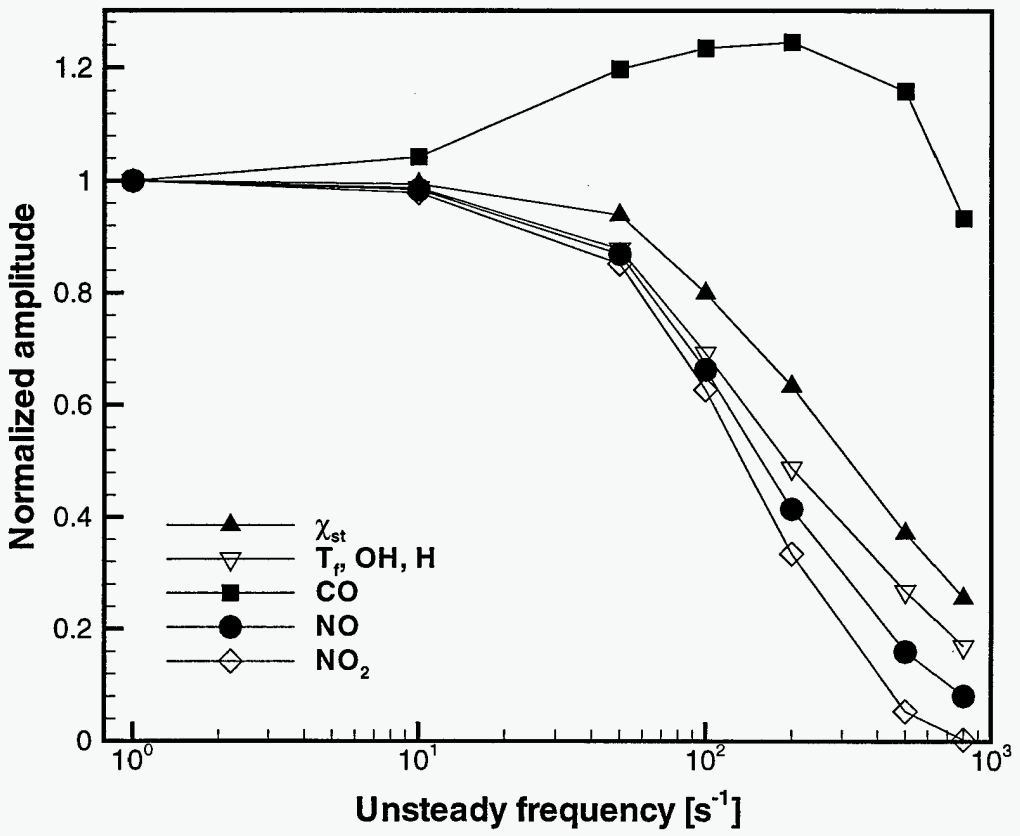

Figure 4: Amplitude of unsteady fluctuation responses normalized by the quasi-steady values as a function of frequency.

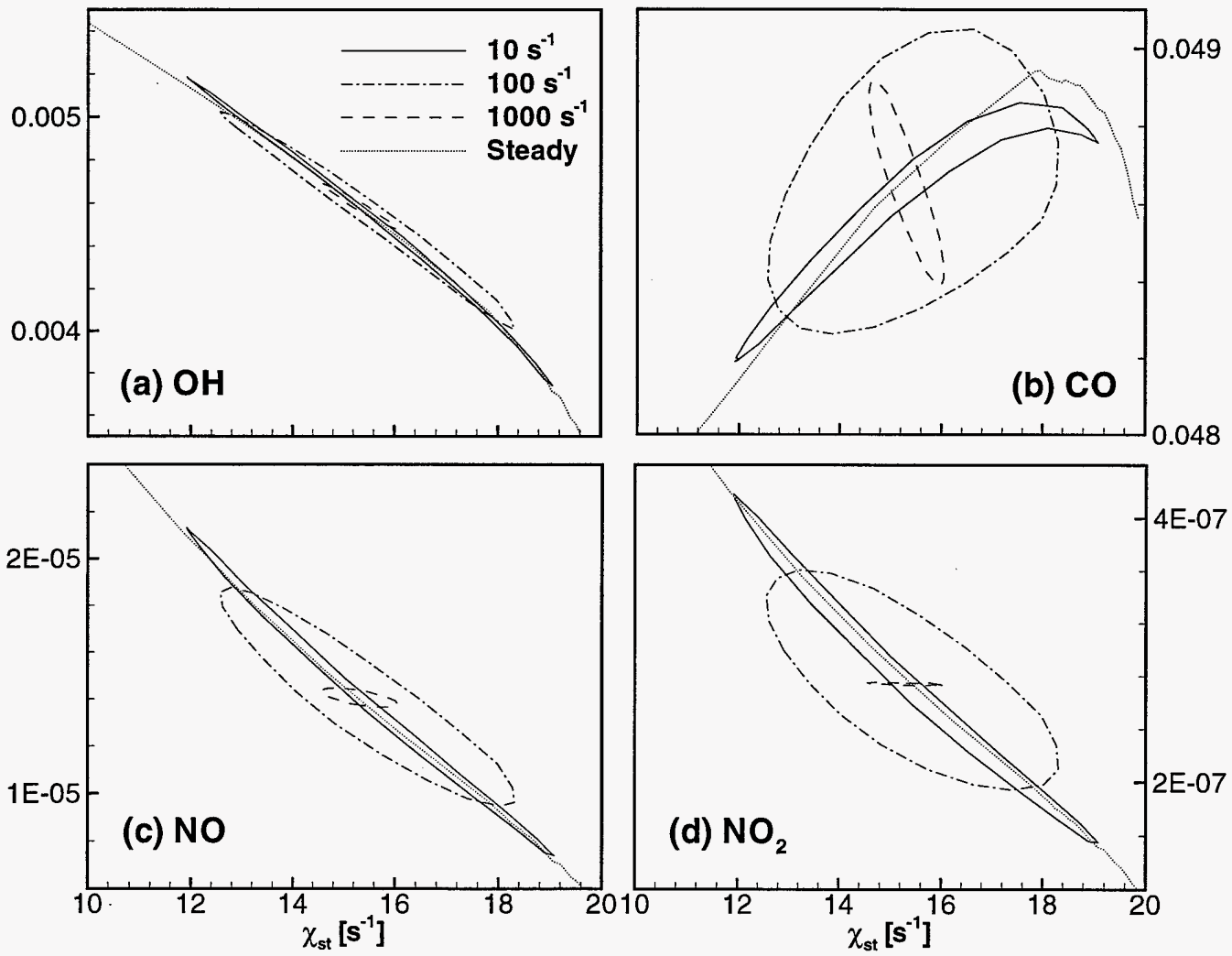

Figure 5: Response of the maximum mole fractions of (a) OH, (b) CO, (c) NO and (d) NO_2 to the scalar dissipation rate, for three different frequencies.

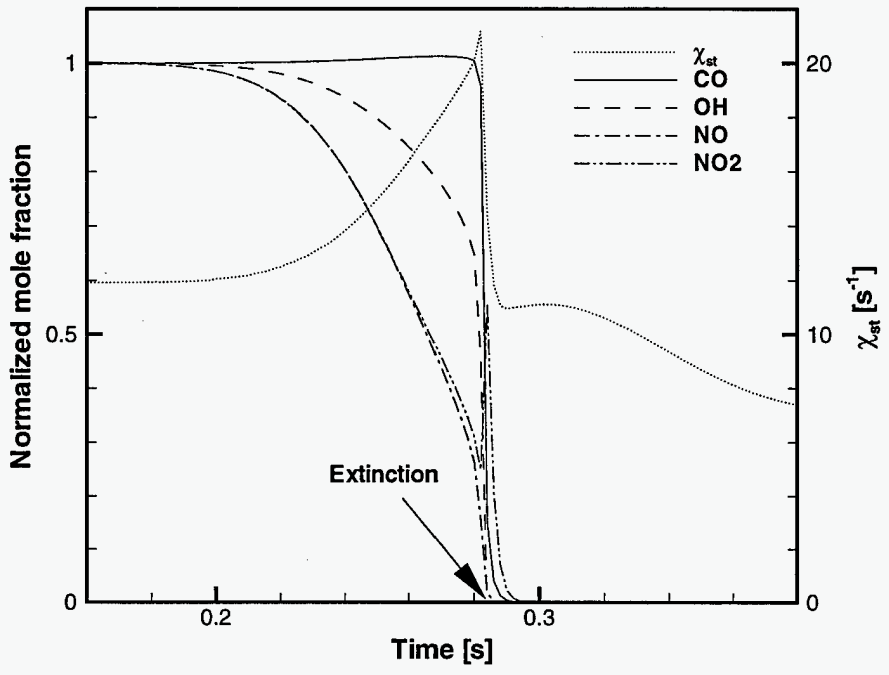

(a)

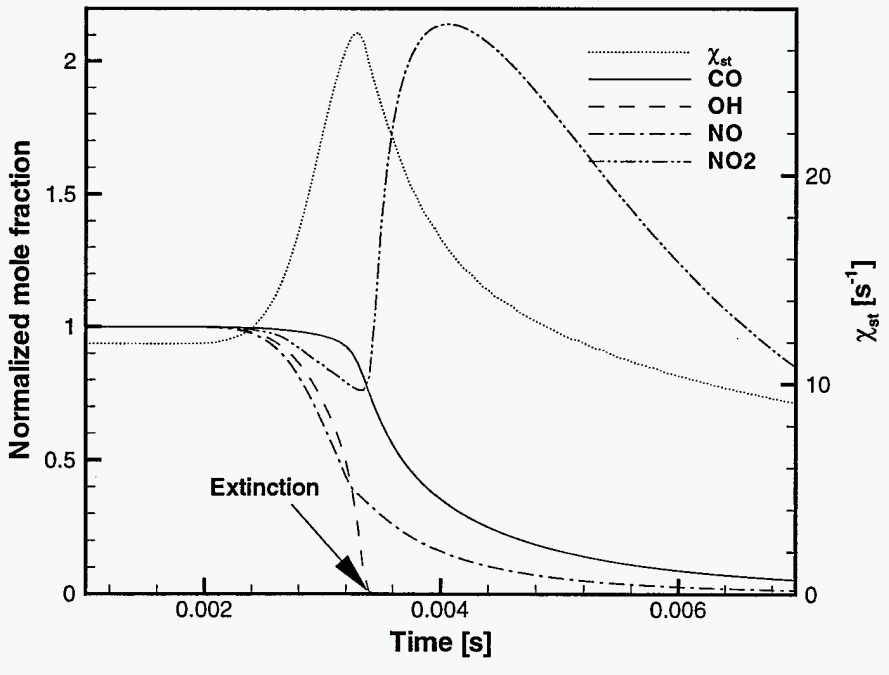

(b)

Figure 6: Response of the scalar dissipation rate and maximum mole fractions of of various species to the impulsive flow field; (a) $u_0 = 100$ cm/s, $A = 0.6$ and $f = 10$ s^{-1}; (b) $u_0 = 100$ cm/s, $A = 2.4$ and $f = 1000$ s^{-1}.

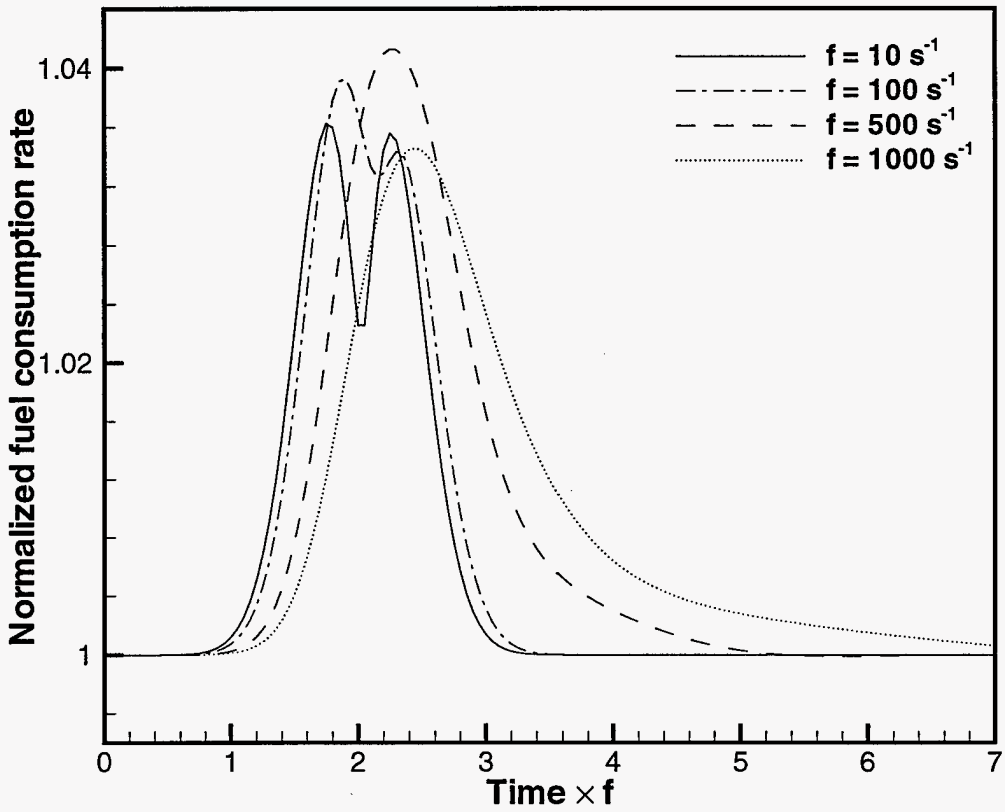

Figure 7: Normalized fuel consumption rate as a function of time for various values of f for $u_0 = 120$ cm/s and $A = 0.23$. The abscissa is normalized by each characteristic time scale.

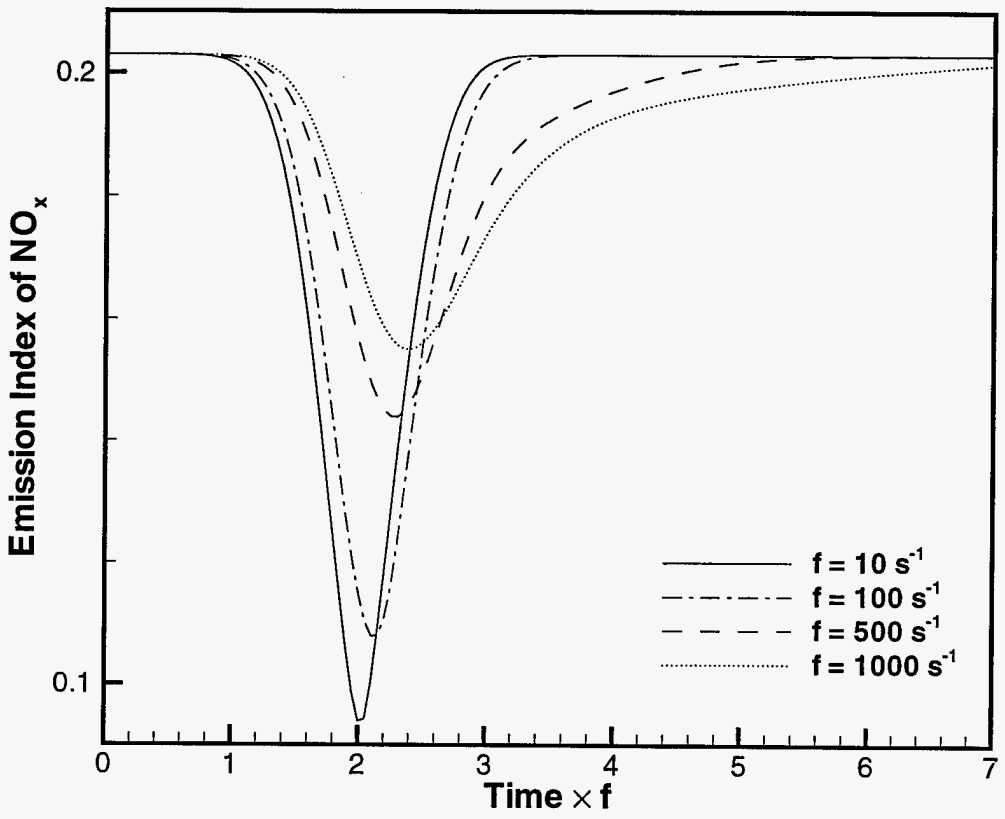

Figure 8: Emission index of NO_x as a function of time for various values of f for $u_0 = 120$ cm/s and $A = 0.23$. The abscissa is normalized by each characteristic time scale.

Report Number (14) SAND--98-8479C
CONF-980804--

Publ. Date (11) 199808
Sponsor Code (18) DOE/EE, XF
UC Category (19) UC-1400, DOE/ER

DOE